Simplified Control Strategies for Power Converters in a Grid-Connected Hybrid DC-AC Microgrid

Simplified Control Strategies for Power Converters in a Grid-Connected Hybrid DC-AC Microgrid

Tiago Davi Curi Busarello, *Senior Member, IEEE*
Department of Control, Automation and Computing Engineering
Federal University of Santa Catarina
Blumenau, Brazil
ORCID: 0000-0002-5406-3811

Marcelo Godoy Simões, *Fellow, IEEE*
School of Technology and Innovations
University of Vaasa
Vaasa, Finland
ORCID: 0000-0003-4124-061X

Hannu Laaksonen, *Member, IEEE*
School of Technology and Innovations
University of Vaasa
Vaasa, Finland
ORCID: 0000-0001-9378-8500

Kimmo Kauhaniemi, *Member, IEEE*
School of Technology and Innovations
University of Vaasa
Vaasa, Finland
ORCID: 0000-0002-7429-3171

***Abstract*—Many typical converter control strategies used in microgrids are complex or require modifications in the power structure. The complexities are due coupling effects among controllers and time-delay caused in exchanging information in the system. This paper proposes simplified control strategies for power converters in a grid-connected hybrid DC-AC microgrid, aiming to ensure precise voltage and current regulation. The used controllers are proportional-resonant, integral-double-lead, proportional-integral and single integral controller. In this paper, the methodology for tuning each controller is carefully described in detail and recommendation for choosing their bandwidth is given. Then, the designed controllers are discretized through the Backward-Euler approximation. The power converters of the microgrid are an inverter, a Buck, a Boost and a bidirectional DC-DC. A case study is conducted through simulations with Matlab/Simulink. Results show that the controlled variables follow their reference signals with negligible steady-state error, proving the efficacy of the simplified control strategies and allowing an stable operation of the microgrid.**

***Index Terms*—Hybrid Microgrid, Power Control, Power Converters, Photovoltaic systems, Battery storage.**

I. Introduction

Accomplishing a microgrid brings several challenges to industries, academia and to the electric sector. Some behaviors that are not commonly found in classical power systems make researchers to seek for solutions that allow a safe realization of microgrids. Some of them are reverse power flow, stability in low-inertia systems and controlling Distributed Energy Resources (DER) accurately.

Microgrids have the feature of being complex due to infinite possible compositions and their inherent time-variant structure. As a consequence, it is not trivial to propose solutions that can be employed to all kinds of microgrids. An attempt to overcome that is to categorize microgrids like AC microgrids, hybrid microgrids, multi-microgrids, among others, and also to define whether they are grid-connected or isolated [1], [2].

One of the most common microgrid configurations is the grid-connected DC-AC hybrid microgrid. The reason behind that is because they have DC and AC buses that can conveniently accommodate Photovoltaic (PV) systems, storage systems and DC and AC loads. Besides that, such a configuration allows a suited energy transactions among the DERs and the main grid.

For the aforesaid type of microgrid, controlling its power converters precisely is somehow mandatory. It ensures that the microgrid operation remains resilient, stable and with uninterruptible supply to loads. Control strategies are constantly reported in the literature. In [3] a strategy to power smoothing and pulse power load accommodation is proposed for a grid-connected PV-hybrid energy storage microgrid. In such a case, the microgrid encompasses hydrogen/bromine redox flow battery and supercapacitor as two storage systems while the control strategy has an antiwindup mixed-order generalized integrator and an improved sparrow search algorithm.

Authors of [4] present a concise revisit of model predictive control strategies for microgrids. The revision covers generalized microgrid configurations and explains how to model and select the best cost functions. The covered strategy is highly dependent on the correct modeling of the microgrid. As stated earlier, the time-variant nature of microgrids imposes a burden in modeling accurately all the phenomena of a microgrid. Another interesting review paper is found in [5], but focusing in stability and control architectures.

Cooperative and coordinated control strategies were proposed in [6], [7]. In [8] an autonomous controller using an interlink converter in a hybrid microgrid is proposed. A similar research that uses an interlink converter is found in [9]. The inclusion of the interlink converters proved to be an engaging solution, but they have the hardship of adding physical components. Other control proposals of hybrid DC-

The authors would like to acknowledge the financial support for the SGFER project provided by the European Regional Development Fund (Regional Council of Ostrobothnia project code: A76338).

AC microgrids can be found in [10], [11].

All of the previous researches have their legitimacy and efficacy. However, either they employ complex control algorithms or require modifications in the physical structure of the microgrid. A more simplified control strategy is needed. Classical controllers can be used, providing good voltage and current regulation as well as guaranteeing stability. This paper proposes simplified control strategies for power converters in a grid-connected hybrid DC-AC microgrid and it is organized as follows. Section II presents the covered microgrid and the control strategy description. Section III describe the methodologies to design each controller while in Section IV simulation results are presented. Conclusions are given in Section V.

II. Microgrid and Control Strategy Description

Fig. 1 presents the microgrid diagram and the simplified control strategies. It has DC and AC bus, a grid-connected three-phase inverter with LCL output filter, a grid with line impedance and three DC-DC converters i.e Boost, Buck and a bidirectional half-bridge leg. All the DC-DC converters are connected to the DC bus. The Boost converter injects power from PV panels into the DC bus. The Buck converter supplies a reduced and highly regulated voltage to DC loads. The bidirectional DC-DC converter interfaces a bank of batteries, allowing the smooth charging and discharging cycles. The AC bus is called Point of Common Coupling (PCC). A communication link is supposed to exist in the microgrid which permits exchanging information among the converters and a microgrid operator.

The measured variables as well as the control strategy block diagram for all power converters are also showed in Fig. 1. The control strategies work independently of each other. The inverter control strategy regulates its output currents ($i_a, i_{,b}, i_c$) and the DC bus voltage (v_{dc}). To do that, the PCC voltage ($v_{pcca}, v_{pccb}, v_{pccc}$) are measured and sent to a Phase-Locked Loop to ensure that the output current is in-phase with the voltage grid. The output current is regulated through Proportional-Resonant (PR) controller in *abc*-reference frame while the DC Bus voltage is regulated using a Proportional-Integrator (PI) controller.

The Boost converter is controlled through an integral controller combined with a resonant filter [12]. The purpose of them is to regulate the voltage (v_{pv}) across the PV panels even in the presence of low-frequency component at the DC Bus. A perturb and observe Maximum Power Point Tracking (MPPT) algorithm is also employed in the Boost control strategy. Such algorithm tracks the maximum point of the convex power function of PV panels under uniform irradiance conditions. The principle of operation of the MPPT algorithm is to give a reference voltage to be applied across the PV panels. If the referred reference voltage results in a power increase, the reference voltage is increased by a value of Δ. Otherwise, the reference voltage is decreased by Δ. This process continues until the MPPT finds the maximum point, which will be stepping around it. A good value for Δ is a few percent of the open-circuit voltage.

For the Buck converter, an integral-double-lead controller is used to control the voltage across the DC load. The bidirectional DC-DC converter employs a PI controller to regulate the current of the battery bank. Such a controller ensures constant-current mode during discharge and charge cycles. An outer voltage controller could be included to allow constant-voltage mode, but it is beyond the scope of this paper.

Even though the control strategy block diagram shows controllers in s-domain, they were implemented in discrete-time domain. Backward Euler discretization was adopted to transfer the controllers to the z-domain.

III. Designing the Controllers

The control strategies described in the previous section are simplified compared to the complex strategies commonly employed in hybrid DC-AC microgrids. The use of classical linear controllers is sufficient to make such a kind of microgrid to operate in stable and consistent manner. Nevertheless, to guarantee that, the controllers must be properly designed. Choosing the appropriate bandwidth for each controller is mandatory for making them to work uncoupled and stable. This section presents the methodology to tune the controllers as well as how to choose the their bandwidth.

The goal of the proposed simplified control strategy is to make a variable, either voltage or current, to follow its reference signal in each converter with negligible steady-state error. The decision of what should be the reference signal is up to the microgrid operator.

A. Controllers of the Inverter

The transfer functions of the output current plant $G_i(s)$ and the PR controller $C_i(s)$ are given respectively by (1) and (2).

$$G_i(s) = \frac{V_{DC}}{L_1 L_2 C s^3 + C L_2 V_{DC} K_a s^2 + (L_1 + L_2)s} \quad (1)$$

$$C_i(s) = K_p + k_i R_{es}(s) \quad (2)$$

where L_1, L_2, C, V_{DC} and K_a are the converter-side inductor, grid-side inductor, capacitor of the LCL filter, DC Bus nominal voltage and active damping coefficient, respectively.

The PR controller are designed by computing (3) and (4) and designing the resonant filter $R_{res}(s)$ given by (5).

$$k_p = \frac{(2\xi + 1)(\sqrt{(2\xi + 1)}\omega_r L_{eq} - R_{eq}}{V_{dc}} \quad (3)$$

$$k_i = \frac{w_r^2 L_{eq}[(2\xi + 1)^2 - 1]}{2V_{dc}} \quad (4)$$

$$Res(s) = \frac{B_r s}{s^2 + 2\zeta B_r s + w_r^2} \quad (5)$$

where $L_{eq} = L_1 + L_2$, R_{eq} means the sum of the resistances of the inductors of the LCL filter, ξ is the damping factor, ω_r is the angular resonant frequency of the grid, B_r is the resonant bandwidth in Hz and ζ is the damping factor of the resonant filter.

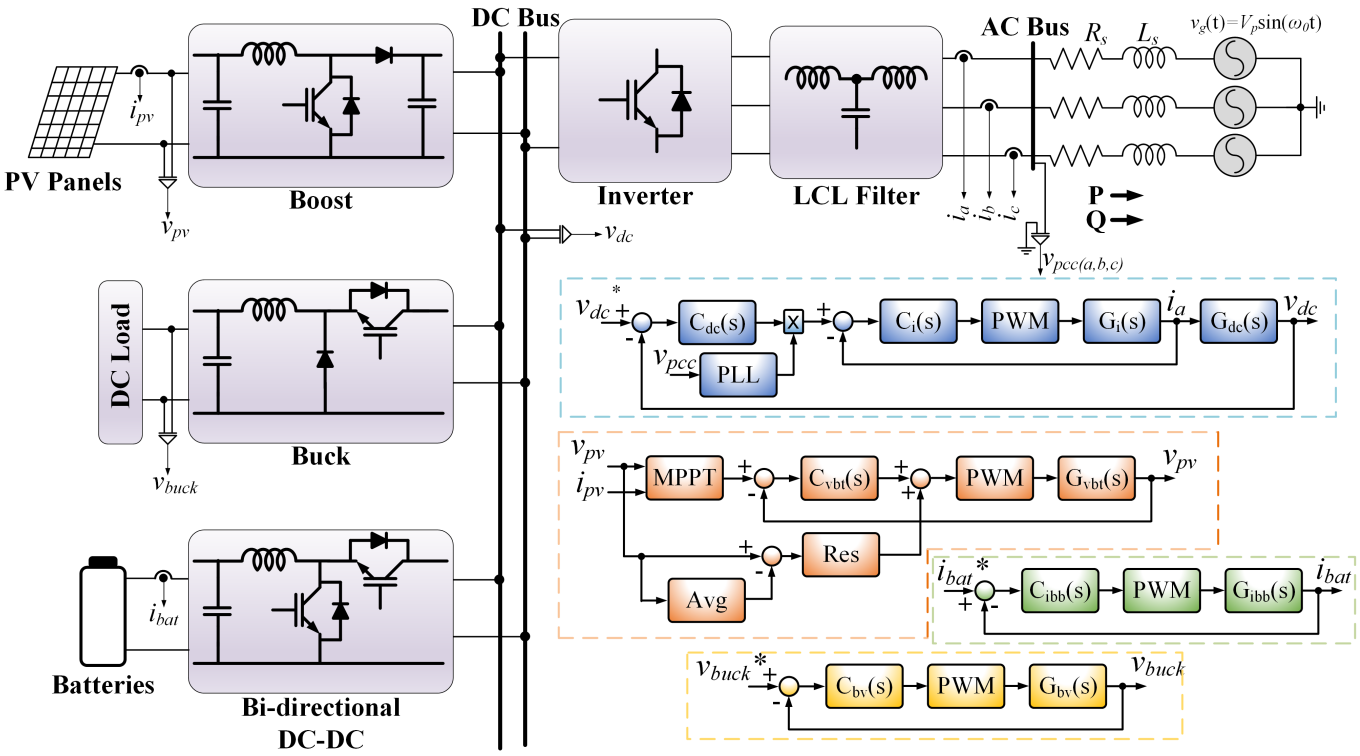

Fig. 1. Microgrid Diagram and the Simplified Control Strategies.

The PR controller must satisfy that its bandwidth is at least ten times lower than the switching frequency. The value of B_r should around $1.5\,Hz$ and ζ any value between 0.1 and 1, where $\zeta = 0.5$ makes the resonant filter to present $0\,dB$ at the resonant frequency.

The transfer functions of the DC bus voltage plant $G_{dc}(s)$ and the DC Bus controller $C_{dc}(s)$ are given respectively by (6) and (7).

$$G_{dc}(s) = \frac{1}{sC_{dc}} \tag{6}$$

$$C_{dc}(s) = \frac{k_{dc}(1 + sT_{dc})}{sT_{dc}} \tag{7}$$

where C_{dc} is the total DC Bus capacitance, k_{dc} is the proportional gain and T_{dc} is the time constant of the controller.

The bandwidth of the DC Bus controller must be chosen at least ten times lower than the bandwidth of the PR controller. Once it is defined, the time constant is established and the parameter of the PI can be easily obtained through the Ziegler–Nichols method.

B. Controller of the Buck Converter

The transfer functions of the voltage plant $G_{bv}(s)$ and the integral-double-lead controller $C_{bv}(s)$ are given respectively by (8) and (9).

$$G_{bv}(s) = \frac{V_{DC}}{s^2 L_f C_f + s\frac{L_f}{R_o} + 1} \tag{8}$$

$$C_{bv}(s) = \frac{n_1 s^2 + (R_2C_1 + R_1C_3 + R_3C_3)s + 1}{(R_1R_2R_3C_1C_2C_3)s^3 + d_2 s^2 + (R_1(C_1 + C_2))s} \tag{9}$$

where $n_1 = R_2C_1C_3(R_1+R_3)$ and $d_2 = R_1R_3C_3(C_1+C_2)+R_1R_2C_1C_2$, L_f, C_f and R_o are the inductance, capacitance and nominal load of the Buck converter.

The bandwidth (f_c) of the integral-double-lead controller must be at least eight times lower than the bandwidth of the DC Bus voltage controller used in the inverter. Besides that, phase margin (PM_d) must be a value within 40° to 80°. After defining them, the controller is tuned by computing (10) to (19).

$$\phi = \angle C_{bv}(f_c) \tag{10}$$

$$G = 10^{\frac{|(C_{bv}(f_c)|}{20}} \tag{11}$$

$$\alpha = PM_d - \phi - 90° \tag{12}$$

$$K = (tan(\frac{\alpha}{4}) + 45°)^2 \tag{13}$$

$$R_1 = 0.01\,(\text{defined}) \tag{14}$$

$$C_2 = \frac{1}{2\pi f_c G R_1} \tag{15}$$

$$C_1 = C_2(K - 1) \tag{16}$$

$$R_2 = \frac{\sqrt{K}}{2\pi f_c C_1} \tag{17}$$

$$R_3 = \frac{R_1}{K - 1} \tag{18}$$

$$C_3 = \frac{1}{2\pi f_c R_3 \sqrt{K}} \tag{19}$$

C. Controller of the Boost Converter

A Boost converter used to interface PV panels has contrary definitions of input and output compared to a boost used to supply elevated voltage to a load. For the microgrid covered in this paper, the input of the Boost is the DC Bus voltage and the output is the voltage across the PV panels. Therefore, the Boost controller must regulate the voltage across the PV panels, resulting in extracting their maximum available power. Such a feature allows the implementation of a single integral controller, given by (20).

$$C_{vbt}(s) = \frac{k_{ib}}{s} \tag{20}$$

Computing k_{ib} starts by plotting the Bode diagram of the voltage-to-control transfer function of the Boost converter. Then, one may obtain the magnitude at a desired cut-off frequency and compute the inversion of it. Equations (21) and (22) describe how to compute k_{ib}.

$$G = 10^{\frac{-\Gamma(s)|_{s \to f_{cb}}}{20}} \tag{21}$$

$$k_{ib} = \frac{1}{G} \tag{22}$$

where $\Gamma(s)$ is the transfer function of the Boost converter and f_{cb} is the desired cut-off frequency.

A resonant controller similar to $R_{res}(s)$ of (5) is employed in the Boost control strategy, but it is tuned at the double of the grid frequency.

D. Controller of the Bidirectional DC-DC Converter

The transfer functions of the current plant $G_{ibb}(s)$ and the the current control $C_{ibb}(s)$ for the bidirectional converter are given respectively by (23) and (24).

$$G_{ibb}(s) = \frac{V_{DC}}{sL_{bb} + R_{bb}} \tag{23}$$

$$C_{ibb}(s) = k_{pbb} + \frac{k_{ibb}}{s} \tag{24}$$

where L_{bb} and R_{bb} are the inductance and resistance of the inductor, respectively.

The parameters of the current controller can be obtained through (25) and (26)

$$k_{pbb} = \frac{L_{bb}}{\tau} \tag{25}$$

$$k_{ibb} = \frac{k_{pbb} R_{bb}}{L_{bb}} \tag{26}$$

where τ is the desired time constant of the controller. Its value should be at least twenty times higher then the sampling period.

IV. Simulation Results

The microgrid of Fig. 1 as well as the proposed control strategies were simulated in Matlab/Simulink. The nominal power of the microgrid is $10\,kW$. The PV panels are a set of 3 parallel strings with 25 modules each. The sampling frequency of the MPPT algorithm is $50\,Hz$ while the switching and sampling frequencies of all converters are $10\,kHz$. The battery bank consist of 40 series connected $7.2\,V$ lithium-ion batteries. Other parameters are listed in Tab. I.

TABLE I
System Parameters

Parameter	Value	Parameter	Value
Inverter			
Grid Voltage (RMS)	$230\,V$	Grid frequency	$50\,Hz$
Grid resistance	$0.01\,\Omega$	Grid inductance	$300\,uH$
DC-Bus voltage	$900\,V$	Conv.-side ind.	$6\,mH$
Resistance of L_1	$0.01\,\Omega$	Grid-side ind.	$1\,mH$
Resistance of L_2	$0.01\,\Omega$	LCL capacitor	$3\,uF$
Resonant bandwidth	$1.5\,Hz$	Resonant freq.	$50\,Hz$
Damping factor	0.975	DC bus time constant	$10\,ms$
Buck			
Inductor	$63\,mH$	Capacitor	$470\,uF$
Load	$45\,\Omega$	Output voltage	$400\,V$
Desired bandwidth	$1\,kHz$	Desired Phase Margin	60°
Boost			
Inductor	$1\,mH$	Capacitor	$470\,uF$
RSE	$0.3\,\Omega$	Resistance of L	$0.04\,\Omega$
Desired bandwidth	$250\,Hz$		
Bidirectional			
Inductor	$15\,mH$	Capacitor	$470\,uF$
Desired time constant	$2\,ms$		

Applying the aforesaid parameters in the methodologies of Section III, all controllers are designed. Then, they are discretized through Backward Euler approximation, resulting in the transfer function given by (27).

$$C_x(z) = C_x(s)|_{s \to \frac{z-1}{zT_s}} = \frac{b_0 + b_1 z^{-1} + b_2 z^{-2} + b_3 z^{-3}}{a_0 + a_1 z^{-1} + a_2 z^{-2} + a_3 z^{-3}} \tag{27}$$

Tab. II presents the coefficients of each designed controller. b_3 is null for all controllers and was omitted.

Fig. 2 presents the active and reactive powers that are injected into the grid. Four intervals are defined, called I, II, III and IV. In interval I, the solar irradiance at the PV panels is increasing, the battery bank is being discharged and the Buck converter is feeding a load with half of its nominal power. The interval II starts when it happens an increase in the solar irradiance (at $t = 5.5\,s$). As a result, more active power is injected into the grid. Interval III starts when the DC load of the Buck converter steps up to full power. At $t = 6.005\,s$, the battery bank changes from discharging to charging mode. The decision of such a time is to make the transition happen at $\pi/2\,rad$ of the PCC voltage, representing the worst scenario for inverting the active power. The power to charge the battery bank and the DC load of the Buck converter is higher than the power generated by the PV panels, leading to a situation in which the grid is supplying power. During all intervals, the reactive power is kept null.

TABLE II
COEFFICIENTS OF THE DESGINED CONTROLLLERS

Controller	b_0	b_1	b_2	a_0	a_1	a_2	a_3
$C_i(z)$	0.9203320202	-1.7891106973	0.8696369743	1.7626129080	-3.5200952333	1.7592186044	0
$C_{dc}(z)$	353.50000000	-350.00000000	0	1	-1	0	0
$C_{bv}(z)$	1.7481457219	-3.2256446654	1.4879742828	1.0000000000	-1.2416301979	0.2775065539	-0.0358763560
$C_{vbt}(z)$	0.00000035500	0	0	4.611686018427388	-4.611686018427384	0	0
$C_{ibb}(z)$	7.5101	- 7.5000	0	1	-1	0	0

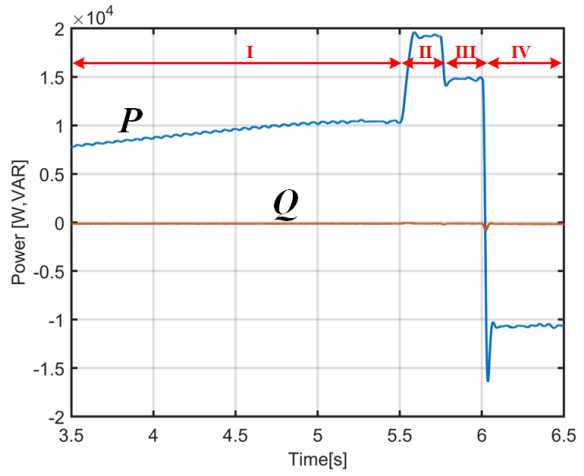

Fig. 2. Grid-injected active and reactive powers.

Fig. 3 presents the PCC voltage, the grid current and DC Bus voltage during all intervals. The grid current is sinusoidal and it does not present unpredictable behavior at any moment. The DC Bus voltage is kept constant during steady-state conditions and present low overshoot during the transitions.

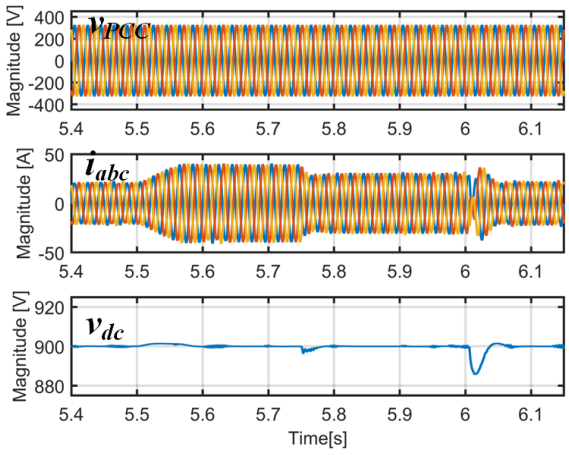

Fig. 3. The PCC voltage, the grid current and DC Bus voltage during all intervals.

Fig. 4 presents the PCC voltage (divided by 3), the grid current and its reference signal during the transition of intervals III and IV. The waveforms are from phase A. Initially, the grid current is synchronized with the PCC voltage. After the transition, the grid-current is in counter-phase related to the PCC voltage, evidencing the consumption of active power by the whole microgrid.

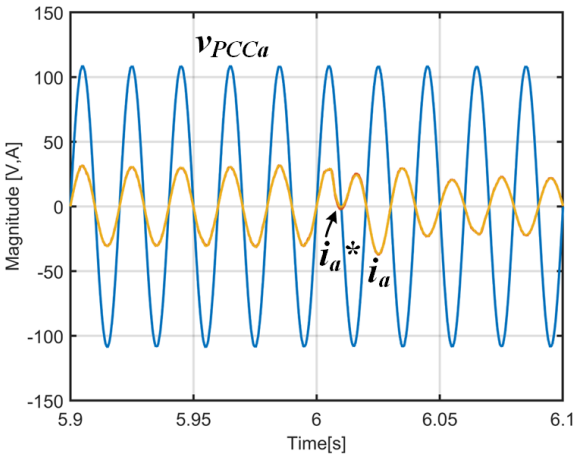

Fig. 4. The PCC voltage (divided by 3), the grid current and its reference signal during the transition of intervals III and IV.

Fig. 5 presents the DC Bus voltage, the output voltage of the Buck converter, its reference signal and the load current. The DC Bus voltage was repeated here for better locating the interval transitions. The output voltage of the Buck converter is controlled at its reference during all intervals, rejecting the perturbations of DC Bus. During transition from intervals II and III, the output voltage suffers a slight oscillation due to the addition of load, but rapidly return to its reference.

Fig. 6 presents results of the boost converter. The voltage across the panels follows its reference signal which comes from the MPPT algorithm. It is also possible to verify that the product of v_{PV} and i_{PV} is coincident with the PV panel power (P_{PV}). At $t = 5.5s$, the irradiance increases from $500\,W/m^2$ to $1000\,W/m^2$. Such increase mimics a situation in which there were clouds causing shadows in the PV panels and suddenly disappeared. Even though this phenomena takes some time to happen, in the simulation a fast change is applied to check the MPPT under the worst-case condition.

Fig. 7 presents the State-of-Charge (SOC) curve and voltage and current of the battery bank. Initially, the battery bank is being discharged at a constant and controlled current of $-20A$. Therefore, the SOC curve decreases. At $t = 6.005\,s$, the battery bank start charging with a $60A$-controlled current. The decision of start charging the battery bank with the SOC curve

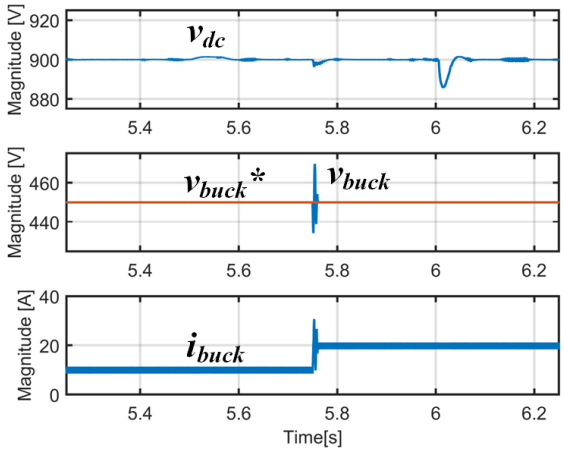

Fig. 5. The DC Bus voltage, the output voltage of the Buck converter, its reference signal and the load current.

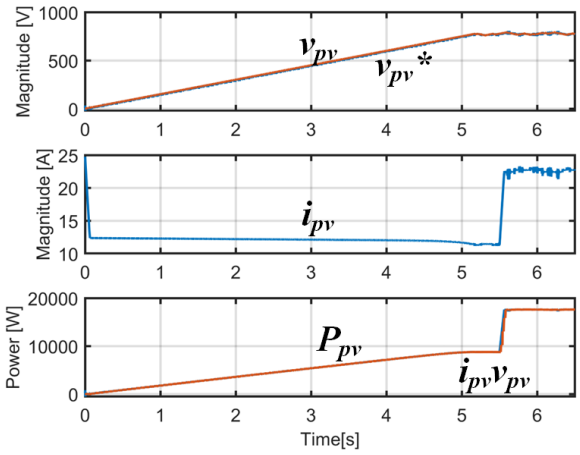

Fig. 6. Results of the Boost converter.

at around 69.8% is just to show a transition in the charging process. Usually, the battery bank starts charging when the SOC is at 30%

V. Conclusions

This paper proposed simplified control strategies for power converters in a grid-connected hybrid DC-AC microgrid. The employment of classical linear controller simplified considerably the voltage and current regulation along the microgrid compared to commonly found complex strategies. The methodology to tune each controller was carefully described, resulting in obtaining all coefficients of their discrete-time transfer functions. Simulations results showed that the controlled variables followed their reference with negligible steady-state error. During transitory intervals, the microgrid did not present any unpredictable behavior. Therefore, the proposed controllers are an attractive solution. For future plans, the proposed strategies provide the basic set of controllers to be applied in the laboratory hardware setup that is being built.

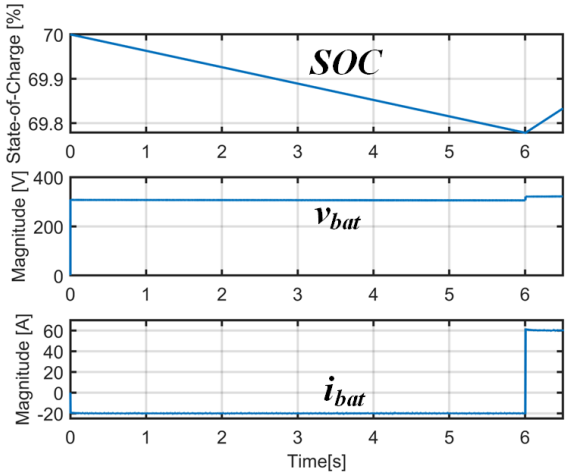

Fig. 7. The State-of-Charge (SOC) curve and voltage and current of the battery bank.

References

[1] Q. Xu, L. Li, X. Chen, Y. Huang, K. Luan, and B. Yang, "Optimal economic dispatch of combined cooling, heating and power-type multi-microgrids considering interaction power among microgrids," *IET Smart Grid*, vol. 2, no. 3, pp. 391–398, 2019.

[2] J. M. Guerrero, P. C. Loh, T.-L. Lee, and M. Chandorkar, "Advanced control architectures for intelligent microgrids—part ii: Power quality, energy storage, and ac/dc microgrids," *IEEE Transactions on Industrial Electronics*, vol. 60, no. 4, pp. 1263–1270, 2013.

[3] M. K. Behera and L. C. Saikia, "A Novel Resilient Control of Grid-Integrated Solar PV-Hybrid Energy Storage Microgrid for Power Smoothing and Pulse Power Load Accommodation," *IEEE Transactions on Power Electronics*, vol. 38, no. 3, pp. 3965–3980, Mar. 2023.

[4] S. Shahzad, M. A. Abbasi, M. A. Chaudhry, and M. M. Hussain, "Model Predictive Control Strategies in Microgrids: A Concise Revisit," *IEEE Access*, vol. 10, pp. 122 211–122 225, 2022.

[5] M. Ahmed, L. Meegahapola, A. Vahidnia, and M. Datta, "Stability and Control Aspects of Microgrid Architectures–A Comprehensive Review," *IEEE Access*, vol. 8, pp. 144 730–144 766, 2020.

[6] A. M. Jasim, B. H. Jasim, V. Bureš, and P. Mikulecký, "A Novel Cooperative Control Technique for Hybrid AC/DC Smart Microgrid Converters," *IEEE Access*, vol. 11, pp. 2164–2181, 2023.

[7] X. Liu, P. Wang, and P. C. Loh, "A Hybrid AC/DC Microgrid and Its Coordination Control," *IEEE Transactions on Smart Grid*, vol. 2, no. 2, pp. 278–286, Jun. 2011.

[8] P. C. Loh, D. Li, Y. K. Chai, and F. Blaabjerg, "Autonomous Control of Interlinking Converter With Energy Storage in Hybrid AC–DC Microgrid," *IEEE Transactions on Industry Applications*, vol. 49, no. 3, pp. 1374–1382, May 2013.

[9] L. Wang, X. Fu, and M.-C. Wong, "Operation and Control of a Hybrid Coupled Interlinking Converter for Hybrid AC/Low Voltage DC Microgrids," *IEEE Transactions on Industrial Electronics*, vol. 68, no. 8, pp. 7104–7114, Aug. 2021.

[10] A. Gupta, S. Doolla, and K. Chatterjee, "Hybrid AC–DC Microgrid: Systematic Evaluation of Control Strategies," *IEEE Transactions on Smart Grid*, vol. 9, no. 4, pp. 3830–3843, Jul. 2018.

[11] Y. Karimi, H. Oraee, and J. M. Guerrero, "Decentralized Method for Load Sharing and Power Management in a Hybrid Single/Three-Phase-Islanded Microgrid Consisting of Hybrid Source PV/Battery Units," *IEEE Transactions on Power Electronics*, vol. 32, no. 8, pp. 6135–6144, Aug. 2017.

[12] G. Viana Silva, H. A. Pereira, T. D. C. Busarello, and A. F. Cupertino, "Estratégia de controle para redução de ondulação de tensão em inversores fotovoltaicos monofásicos de dois estágios," in *IX Congresso Brasileiro de Energia Solar*, 2022, pp. 1–10.